Accepted Manuscript

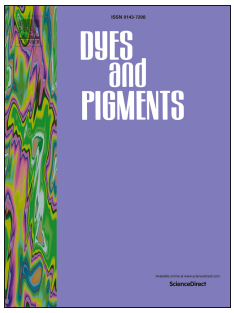

An unusual AIE fluorescent sensor for sequentially detecting Co^{2+}-Hg^{2+}-Cu^{2+} based on diphenylacrylonitrile Schiff-base derivative

Jiabin Qiu, Shengjie Jiang, Bingni Lin, Hongyu Guo, Fafu Yang

PII: S0143-7208(19)30894-0

DOI: https://doi.org/10.1016/j.dyepig.2019.107590

Article Number: 107590

Reference: DYPI 107590

To appear in: *Dyes and Pigments*

Received Date: 22 April 2019

Revised Date: 26 May 2019

Accepted Date: 27 May 2019

Please cite this article as: Qiu J, Jiang S, Lin B, Guo H, Yang F, An unusual AIE fluorescent sensor for sequentially detecting Co^{2+}-Hg^{2+}-Cu^{2+} based on diphenylacrylonitrile Schiff-base derivative, *Dyes and Pigments* (2019), doi: https://doi.org/10.1016/j.dyepig.2019.107590.

An unusual AIE fluorescent sensor for sequentially detecting Co^{2+}-Hg^{2+}-Cu^{2+} based on diphenylacrylonitrile Schiff-base derivative

Jiabin Qiu,[a] Shengjie Jiang,[a] Bingni Lin,[a] Hongyu Guo,*[a,b] and Fafu Yang*[a,c]

[a]*College of Chemistry and Materials, Fujian Normal University, Fuzhou 350007, P. R. China ;Tel: +0086-591-83465225; E-mail: yangfafu@fjnu.edu.cn*

[b]*Fujian Key Laboratory of Polymer Materials, Fuzhou 350007, P. R. China*

[c]*Fujian provincial Key Laboratory of Advanced Materials Oriented Chemical Engineering, Fuzhou 350007, P. R. China*

Aggregation-induced emission (AIE) molecules with strong fluorescence in aggregated states are favorable for preparing the organic fluorescence sensor in aqueous phase. In this work, a red fluorescent sensor **5** based on AIE diphenylacrylonitrile Schiff-base derivative was prepared in yield of 83.7%. Sample **5** exhibited strong AIE property in water with red fluorescence at λ_{ex} = 620 nm and the Stokes shift was as large as 260 nm. The experiments of sensing series of metallic ions suggested that sample **5** possessed the sequentially detecting abilities for Co^{2+}-Hg^{2+}-Cu^{2+}, which was observed firstly for organic fluorescence sensor. The fluorescence of sample **5** was quenched rapidly in presence of Co^{2+}, then recovered by adding Hg^{2+} and quenched once more by further adding Cu^{2+}. The detection limits for Co^{2+}, Hg^{2+} and Cu^{2+} were 0.0937, 0.0221, and 0.0988 μM, respectively. The sensor mechanism was confirmed by fluorescence titration, ^{1}H NMR and MS spectra, indicating the 2:1 stoichiometric ratios of sample **5** with ions. The sensor for ions was successfully applied in test paper, exhibiting good practical application potential for detecting Co^{2+}-Hg^{2+}-Cu^{2+} sequentially. Sample **5** showed good bioimaging performance on living cell. The fluorescence of living cells with sample **5** also displayed the similar change of quenching-recovering-quenching by adding Co^{2+}-Hg^{2+}-Cu^{2+} orderly, implying the good ions-detecting prospect in living body environment.

Keywords: Diphenylacrylonitrile; Fluorescence; Sensor; Co^{2+}; Hg^{2+}; Cu^{2+}

1. Introduction

Contamination of heavy metals seriously threatens to human's health and causes series of diseases usually [1,2]. For instance, copper induces Menkes syndrome, cobalt leads to radiation skin damages, and mercury disturbs the central neural system [3-5]. Thus, it is very important to develop the timely and efficient detection method for heavy metals ions among all kinds of complicated environment such as mine

wastewater, industrial sewage, even living organisms. Traditional detection methods including atomic absorption spectroscopy (AAS), atomic fluorescence spectrometry (AFS), X-ray fluorescence spectrographic (XFS) and inductively coupled plasma mass spectrometry (ICP-MS) [6,7], are successfully used in heavy metals detection. However, although those testing instruments are sensitive and accurate in general, they were restricted for its huge equipment, complex and professional operation.

Recently, the fluorescent sensors attracted much attention in detecting ions due to their obvious advantages of high sensitivity, low cost, and simple operation [8-13]. Many traditional dye molecules with excellent photoluminescence, such as BODIPY, fluorescein dyes, rhodamine dyes and cyanine dyes were modified as excellent fluorescent probes for sensing anionic ions, cation ions, biological molecules, etc [14-21]. These fluorescent probes have been usually studied in organic solvents or organic/aqueous mixtures solutions, limiting their practical application due to the strong aggregation-caused quenching (ACQ) effect in aqueous solution. In 2001, Tang's group reported the aggregation induced emission (AIE) phenomenon for the first time [22]. AIE molecules can effectively eliminate the ACQ effect, resulting in the widely application in numerous fields**,** such as luminous liquid crystal [23-26], organic light-emitting diodes (OLED) [27-29], circularly polarized photoluminescence [30-32], ion detection and biomolecular recognition in water [33-42].

Usually, both the traditional dye probes and AIE probes exhibited the selectively sensing abilities for one kind of metallic ions. Obviously, the selective sensor for multiple metallic ions has the advantage of higher efficiency, cheaper cost and more simplified operation in comparison with the sensor for one metallic ion. Up to now, few examples involved the sensing abilities for two kinds of metallic heavy ions, such as for Hg^{2+} and Ag^{+}, Zn^{2+} and Cd^{2+}, or Fe^{3+} and Hg^{2+} [20, 43, 44]. In this paper, we wish to report an unusual AIE fluorescent sensor for three kinds of heavy ions for the first time. This sensor was a simple diphenylacrylonitrile Schiff-base derivative, exhibiting the sequentially detecting abilities for Co^{2+} with fluorescence quenching, Hg^{2+} with fluorescence enhancement, and Cu^{2+} with fluorescence quenching again. Moreover, it was successfully applied in test paper and bioimaging.

2. Experimental

2.1 General

All chemical reagents were obtained from J&K Chemicals and were used directly. TLC analysis was carried out on pre-coated glass plates. Silica gel (200-300 mesh) was used for the purification of rapid column chromatography. NMR spectra were recorded on a Bruker-ARX 400 instrument at 26 ^{o}C. MS spectra were examined on Bruker mass spectrometer. UV-Vis spectra were measured on Varian UV-Vis spectrometer. Fluorescence spectra were investigated in a conventional quartz cell (10×10×45 nm) on a Hitachi F-4500 spectrometer at 26 ^{o}C. The fluorescence absolute Φ_F values were obtained on FLS920 Fluorescence spectrometer with a 6-inch integrating sphere. The MCF-7 cancer cells were supplied by the school of Pharmacy, Fujian Medical University.

*2.2. Synthetic procedure for compound **3***

Under the protection of nitrogen, 4-hydroxybenzaldehyde (2.43 g, 15 mmol) and 4-nitrophenylacetonitrile (1.83 g, 15 mmol) were dissolved in 100 mL of dry dichloromethane with 1.5 mL of piperidine in the reaction solution. The mixture was stirred at room temperature for 5 h. The colour of the solution changed to a burgundy, accompanying with brown precipitation. When all of the starting materials disappeared by the TLC detection, the reaction was stopped and neutralized with 10% of dilute hydrochloric acid. The organic layer was partitioned and the solution was distilled. The residue was recrystallized in $CHCl_3$-MeOH and compound **3** was obtained as yellowish solid in yield of 87.6%. ^{1}H NMR (400 MHz, $CDCl_3$): δppm: 13.03 (d, *J* = 12.0 Hz, 2H, ArH), 12.83 (s, 1H, C=CH), 12.68 (d, *J* = 12.0 Hz, 2H, ArH), 12.63 (d, *J* = 12.0 Hz, 2H, ArH), 11.63 (d, *J* = 12.0 Hz, 2H, ArH), 9.45 (bs, 1H, OH). MALDI-TOF-MS ($C_{15}H_{10}N_2O_3$) calcd for m/z = 266.0691, found: m/z = 266.0664 (M^+).

*2.3 Synthetic procedure for compound **4***

In nitrogen atmosphere, compound **3** (2.66 g, 10 mmol) and urotropin (2.80 g, 20 mmol) were dispersed in 30 mL of trifluoroacetic acid. The mixture was stirred and refluxed for 12 h. TLC detection suggested the dissapearance of materials. Then trifluoroacetic acid in the reaction system was evaporating by vacuum distillation, and the residues were further separated and purified by chromatographic silica gel column (eluent: dichlormethane/petroleum ether = 3:1). Compound **4** was collected in yield of 46.3% as orange solid. ^{1}H NMR (400 MHz, DMSO-d_6), δppm: 13.08 (s, 1H, ArH), 13.06 (d, *J* = 8.0 Hz, 2H, ArH), 13.00 (s, 1H, CHO), 12.93 (d, *J* = 8.0 Hz, 1H, ArH), 12.73 (d, *J* = 8.0 Hz, 2H, ArH), 12.51 (s, 1H, C=CH), 11.92 (d, *J* = 8.0 Hz, 1H, ArH), 8.12 (bs, 1H, OH). HR-MS (ESI) ($C_{16}H_{10}N_2O_4$) Anal. calcd: 294.0641. Found: 294.0632.

*2.4 Synthetic procedure for compound **5***

Under the protection of nitrogen, compound **4** (0.59 g, 2 mmol) with 2-aminopyridine (0.19 g, 2 mmol) were dissolved in 20 mL of MeOH with five drops of glacial acetic acid as catalyst. The mixture was stirred and refluxed overnight and the dark red precipitate appeared. After evaporating the solvent under vacuum distillation, the residue was purified with recrystallization in MeOH. The target compound **5** was obtained as blood-red solid in yield of 83.7%. ^{1}H NMR (400 MHz, DMSO-d_6), δppm: 10.34 (s, 1H, N=CH), 8.36 (s, 1H, ArH), 8.33 (d, *J* = 8.0 Hz, 2H, ArH), 8.25 (s, 1H, C=CH), 8.18 (d, *J* = 8.0 Hz, 1H, ArH), 8.01 (d, *J* = 8.0 Hz, 2H, ArH), 7.87 (bs, 1H, ArH), 7.34-7.38 (m, 1H, ArH), 7.15(d, *J* = 12.0 Hz, 1H, ArH), 6.43-6.48 (m, 2H, ArH), 5.89 (bs, 1H, OH). ^{13}C NMR (100 MHz, DMSO-d_6), δppm: 190.14, 164.28, 159.93, 149.54, 147.32, 145.63, 140.88, 137.69, 137.09, 131.35, 126.99, 124.73, 123.32, 120.27, 118.95, 117.86, 112.32, 108.62, 105.68. HR-MS (ESI) ($C_{21}H_{14}N_4O_3$) $[MH]^+$: Anal. calcd: 371.1146(MH^+). Found: 371.1189(MH^+).

2.5 MTT Assay

Methylthiazolyldiphenyl-tetrazolium (MTT) trials were done to determine the toxicity for MCF-7 cancer cells. The Inoculated MCF-7 cancer cells were cultivated at 37 ^oC and 5% CO_2 for 24 hours, then 1.0×10^{-5} M of sample **5** was tracked in the cells after incubating for 24 h. The fostered cells were rinsed by PBS buffer, and continue cultivating for 3 hours, in 0.5 mg/mL MTT-PBS buffer. Further, 100 μL of

DMSO was added into dissolve the generated Formazan crystals, and detected the absorption intensity at 490 nm.

2.6 The experiment of living cell imaging

Compound **5** (3.0 mg) was dissolved in 1 mL of DMSO and then diluted with PBS buffer (pH = 7.4) to concentration of 1.0×10^{-5} M for imaging test. MCF-7 cancer cells were cultivated at the above identical circumstance of MTT trials for 24 h, and then being tinted by 1.0×10^{-5} M of sample **5** with 24 h breeding. After rinsing with PBS-buffer, dyed cells were cultivated in solution of metallic ions (1.0×10^{-5} M) for 1 hour at 37 ^{o}C, respectively. The cells were imaged by a confocal laser scanning microscope (CLSM, Zeiss LSM 710, Jena, Germany).

3. Results and discussion

3.1. Synthesis and characterization

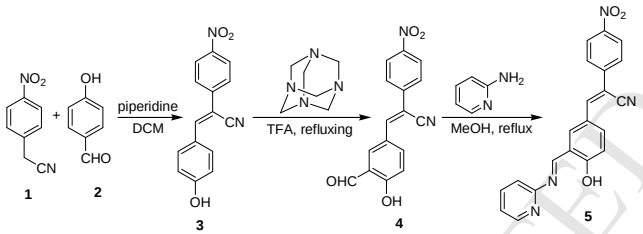

Scheme 1 The synthetic route for target compound **5**

In order to sense heavy ions effectively, the target compound was designed by introducing the pyridine unit, Schiff-base group and phenolic group into diphenylacrylonitrile skeleton to produce the multiple N and O binding sites for metallic ions. The nitrophenylacetonitrile was used for increasing the molecular polarity, which was in favour of the long-wavelength fluorescence. The synthetic route was illustrated in Scheme 1. Briefly, the diphenylacrylonitrile derivative **3** was prepared in yield of 87.6% at room temperature by condensation of 4-hydroxybenzaldehyde and 4-nitrophenylacetonitrile in dry dichloromethane, with equal molar ratio of piperidine as catalyst. Compound **3** was further converted to compound **4** in yield of 46.3% via the classic Duff-reaction under the refluxing reaction system of hexamethylenetetramine and trifluoroacetic acid. Finally, the target compound **5** was synthesized by the Schiff-base condensation of compound **4** and 2-amino pyridine. The yield was as high as 83.7% after recrystallization. The structure of target compound **5** was confirmed by ^{1}H NMR, ^{13}C NMR, and HR-MS spectral analyses (see the ESI). The molecular ion peak $(MH)^{+}$ at 371.1189 in the HR-MS spectra agreed well with the accurate value of the molecular weight of compound **5**. The signals of the ^{1}H NMR spectra and ^{13}C NMR spectra were also in accordance with the structure.

3.2. AIE properties

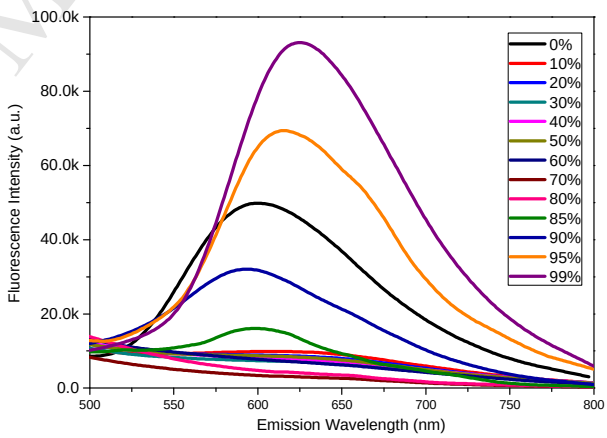

Figure 1. Fluorescence spectra of sample **5** (1 μM) in THF and THF-H_2O mixtures with different water fractions, λ_{ex} = 360 nm.

The AIE properties of compound **5** were studied by UV and photoluminescence spectra in THF-H_2O mixtures. Figure 1 illustrated the corresponding fluorescent spectra in THF-H_2O

mixtures and the plot of fluorescence intensities versus the water fractions was displayed in Figure 2. It can be seen that sample **5** exhibited certain fluorescence intensity in pure THF, which decreased rapidly with the increase of H_2O fractions and kept at the low levels when f_{water} < 80%. As f_{water} > 80%, the fluorescence intensities enhanced dramatically. The fluorescence intensity at f_{water} = 99% was 30 times higher than that in 70% of water fraction. The particle size distribution of sample **5** (1 μM) in solution of THF-H_2O (1:99) was also evaluated by dynamic light scattering (DLS). The results suggested that the average size distribution of sample **5** were 100 nm (Figure S6). The outstanding fluorescence in solid state was also observed for sample **5** as shown in Figure S7. Moreover, the fluorescence quantum yields of sample **5** in pure THF solution, THF-H_2O with 99% of water fractions and solid state were determined as 1.1%, 24.6% and 26.8%, respectively. These results certainly implied the strong AIE effect for sample **5** in aggregated state. On the other hand, the maximum fluorescence wavelength showed some red shift with the increase of water fractions. These phenomena could be explained by the TICT effect due to the electron-donating abilities of the hydroxyl group and the electron-withdrawing abilities of the cyano and nitro group. Based on this strong molecular polarity, sample **5** exhibited the rose-bengal luminescence with emission wavelength at 620 nm and the Stokes shift was as large as 260 nm (as shown in Figure S8), which was seldom observed for diphenylacrylonitrile derivative. The strong long-wavelength fluorescence with large Stokes shift was favourable for the detection due to its advantages of deep tissue infiltration, minimal self-absorption, low background noise and high signal-to-noise ratio of biological resources [45].

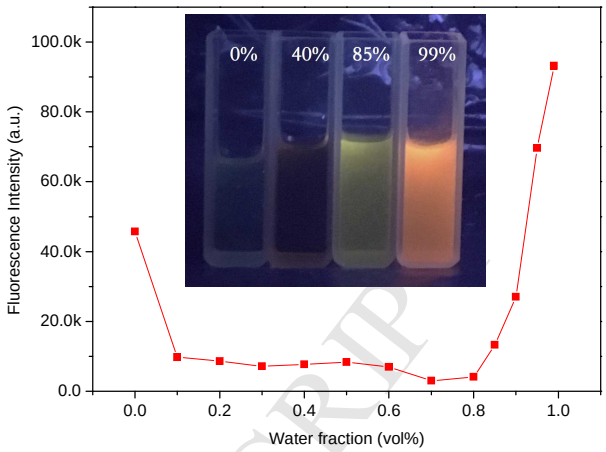

Figure 2. Plot of fluorescence intensities versus the water fractions of THF-H_2O mixtures. Insert: The fluorescence images of sample **5** (1 μM) in THF-H_2O with water fractions of 0%, 40%, 85% and 99%, respectively.

3.3 The sensor for metallic ions

The sensor abilities of compound **5** for metallic ions were investigated by measuring the fluorescence change of sample **5** with all kinds of cations. As shown in Figure 3, the fluorescences of sample **5** were little influenced by Ag^+, Al^{3+}, Ba^{2+}, Bi^{3+}, Fe^{3+}, Hg^{2+}, K^+, Mg^{2+}, Na^+, Ni^{2+}, Pb^{2+}, Zn^{2+}, Cr^{2+}, Ca^{2+}, Li^+ and Cd^{2+} with the small fluctuation of fluorescence intensity. The fluorescence wavelength of sample **5** with Ag^+ and Hg^{2+} exhibited a little blue shift, which could not be distinguished by naked eye. However, it could be seen that the fluorescence of sample **5** after binding with Co^{2+} and Cu^{2+} exhibited strong fluorescence quenching. The fluorescence was almost invisible (inserted picture of Figure 5). These results suggested that sample **2** was an excellent sensor for Co^{2+} and Cu^{2+}.

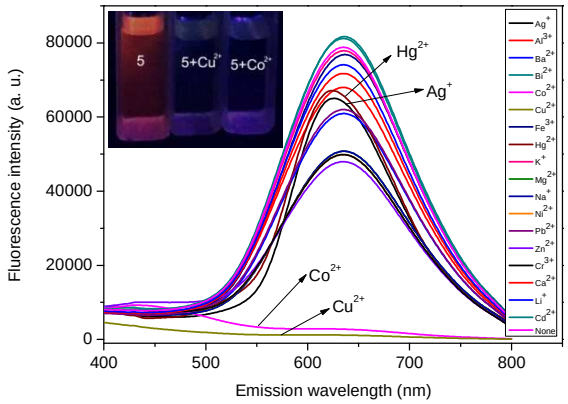

Figure 3. Fluorescence spectra of sample **5** (0.1 μM) with different metal cations (0.1 μM) in THF-H_2O mixtures with 99% of water fractions. λ_{ex}= 360 nm.

3.4 Titration of Co^{2+} and Cu^{2+}

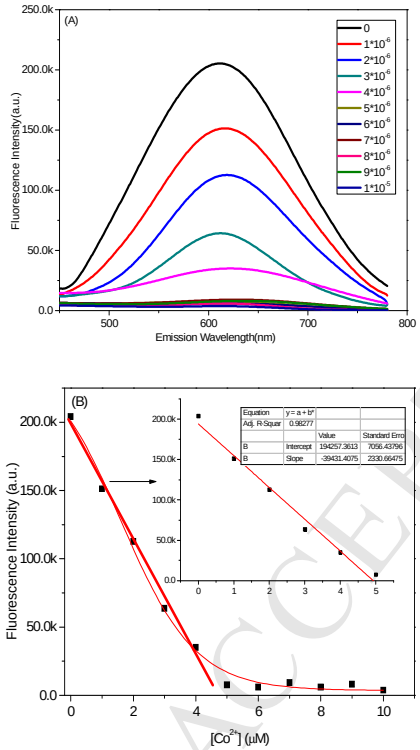

Figure 4. (A) Fluorescence spectra of sample **5** (10 μM) with different concentrations of Co^{2+} in THF-H_2O (1:99), λ_{ex} = 360 nm. (B) The fluorescence intensities of probe titration with Co^{2+}.

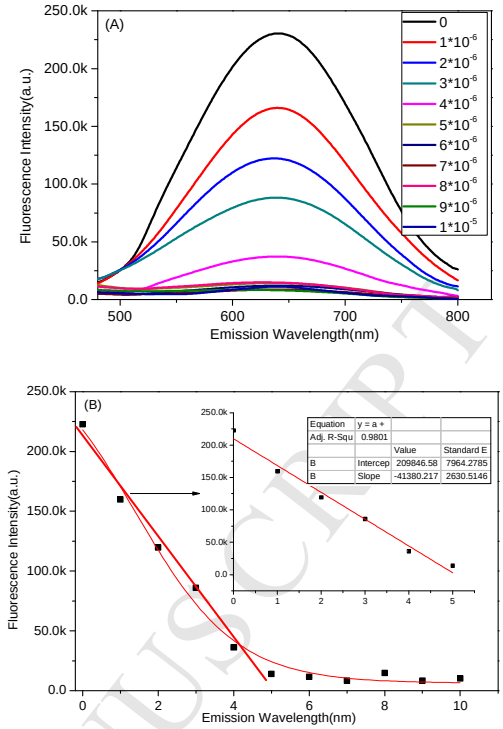

Figure 5. (A) Fluorescence spectra of sample **5** (10 μM) with different concentrations of Cu^{2+} in THF-H_2O (1:99), λ_{ex}= 360 nm. (B) The fluorescence intensities of probe titration with Cu^{2+}.

The further investigation of the sensing properties of sample **5** for Co^{2+} and Cu^{2+} were carried out by the fluorescence titration experiments. As shown in Figure 4(A) and 5(A), with the increase of the concentration of Co^{2+} or Cu^{2+}, the intensities of the emission of sample **5** decreased rapidly and the fluorescence was almost quenched completely when 0.5 equiv of Co^{2+} or Cu^{2+} was added in. These results might indicate the 2:1 of stoichiometric ratio for sample **5** with Co^{2+} or Cu^{2+}, which was further confirmed by the following work. Based on the changes of fluorescence spectra, the corresponding plot of fluorescence intensities versus concentrations of Co^{2+} or Cu^{2+} was illustrated in Figure 4(B)

and 5(B), respectively. It can be seen a good linear relationship for the systems with 0.0 to 5.0 μM metallic ions. According to the calculation formula DL = K × Sb1/S (where K = 2 or 3, in this case the value = 2, Sb1 is the standard deviation of the blank solution, S is the value of the slope of the regression line), the detection limit can be calculated as DL = 0.0937 μM for Co^{2+} and 0.0894 μM for Cu^{2+}, respectively.

3.5 Interference experiments

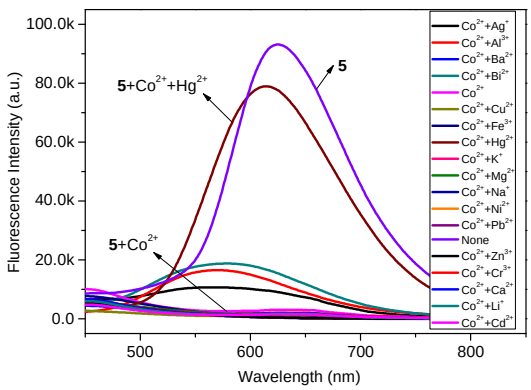

Figure 6. Fluorescence spectra of sample **5** (1 μM), sample **5** and Co^{2+}(1 μM) or Co^{2+}(1 μM) along with other species (1 μM) in THF-H_2O (1:99), λ_{ex} = 360 nm.

To study the interference of other cations, the sensing selectivity of sample **5** for Co^{2+} and Cu^{2+} were investigated by competition experiments with other metal ions. The results were exhibited in Figure 6 and 7. It can be seen that, sample **5** and Co^{2+} with other metallic ions maintained fluorescence quenching or weak fluorescence except Hg^{2+}. The fluorescence almost completely restored for sample **5** with Co^{2+} and Hg^{2+}. The maximum wavelength displayed a little blue shift as in previous sensing experiment. This result suggested the system of sample **5** + Co^{2+} possessed the selectively sensing abilities for Hg^{2+}. As to the system of sample **5** + Cu^{2+}, the fluorescence quenching could not be influenced by adding other metallic ions as shown in Figure 7.

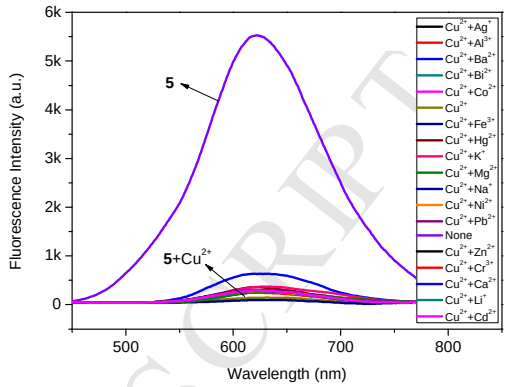

Figure 7. Fluorescence spectra of sample **5** (1 μM), sample **5** and Cu^{2+}(1 μM) or Cu^{2+}(1 μM) along with other species (1 μM) in THF-H_2O (1:99), λ_{ex} = 360 nm.

3.6 The sequentially sensor for Co^{2+}-Hg^{2+}-Cu^{2+}

As the interference experiments suggested the fluorescence of sample **5** + Co^{2+} could be lightened by adding Hg^{2+} but the fluorescence of sample **5** + Cu^{2+} had no the same phenomenon, thus, the unusual fluorescent sensor for sequentially detecting Co^{2+}-Hg^{2+}-Cu^{2+} could be constructed based on these results. The sequentially detecting procedure for detecting Co^{2+}-Hg^{2+}-Cu^{2+} was illustrated in Figure 8. The red fluorescence was firstly quenched in presence of Co^{2+} and then lightened again by adding Hg^{2+}. After Cu^{2+} was further added in, the fluorescence was quenched once more. Based on these phenomena, the sequentially sensor for Co^{2+}-Hg^{2+}-Cu^{2+} were studied by the fluorescence titration experiments.

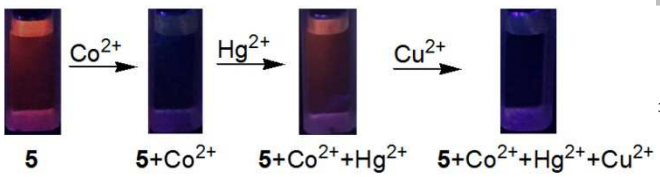

Figure 8. The changes of fluorescent photos of sample **5** for sequentially detecting Co^{2+}-Hg^{2+}-Cu^{2+} (under UV light, 365 nm)

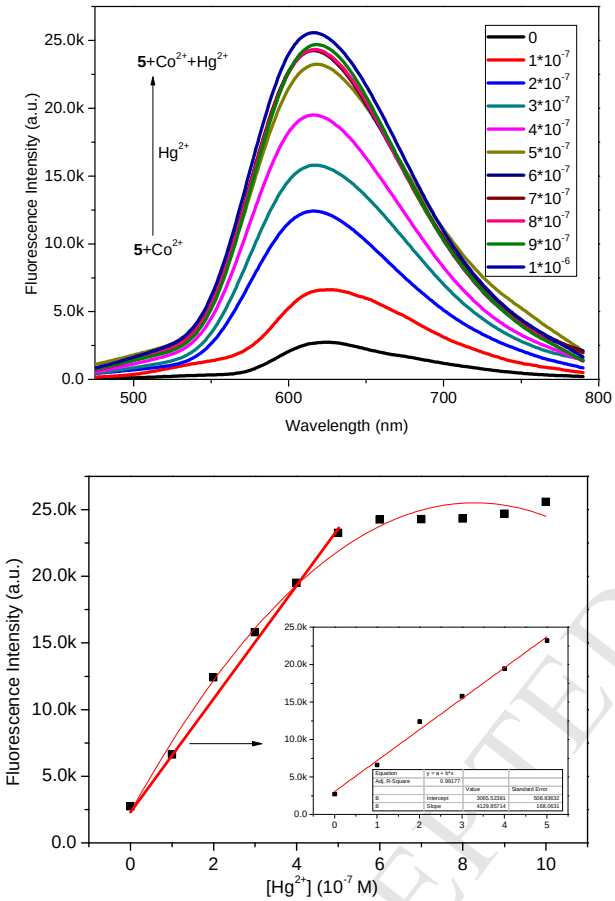

Figure 9. (A) Fluorescence spectra of sample **5** (1 μM) + Co^{2+} (1 μM) with different concentrations of Hg^{2+} in THF-H_2O (1:99), λ_{ex}= 360 nm. (B) The fluorescence intensities of probe titration with Hg^{2+}.

As shown in Figure 9(A), with the increase of the concentration of Hg^{2+}, the intensities of the emission of the system of sample **5** and Co^{2+} enhanced rapidly and attained the maximum value at about 0.5 μM of Hg^{2+}, which might suggest 2:1 of stoichiometric ratio for sample **5** with Hg^{2+}. Figure 9(B) illustrated the corresponding plot of fluorescence intensities versus concentrations of Hg^{2+}. A good linear relationship for the systems with 0.0-0.5 μM of Hg^{2+} could be observed. The detection limit could be calculated as 0.0221 μM for Hg^{2+} according to the previously mentioned calculation formula DL = K × Sb1/S.

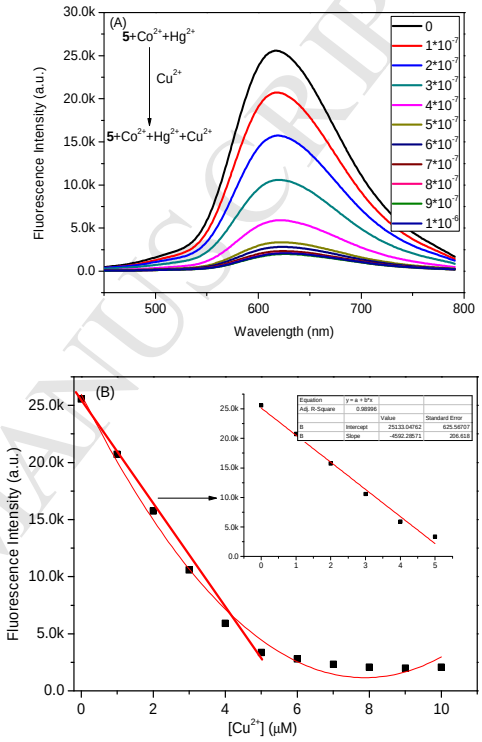

Figure 10. (A) Fluorescence spectra of sample **5** (1 μM) + Co^{2+} (1 μM) + Hg^{2+} (1 μM) with different concentrations of Cu^{2+} in THF-H_2O (1:99), λ_{ex}= 360 nm. (B) The fluorescence intensities of probe titration with Cu^{2+}.

Furthermore, the mixture systems of sample **5**, Co^{2+} and Hg^{2+} were treated with different concentrations of Cu^{2+}. The fluorescence was quenched gradually once more with the increase of concentration of Cu^{2+} as shown in Figure 10. The turning point for fluorescence change also appeared at 0.5 μM

of Cu^{2+}, indicating the 2:1 of stoichiometric ratio for sample **5** with Cu^{2+} again. According to calculation formula DL = K × Sb1/S, the detection limit was calculated as 0.0938 μM for Cu^{2+}. This value was a little bigger than that of the previous system of sample **5** with Cu^{2+} (0.0894 μM). The difference might be attributed to the influence of Co^{2+} and Hg^{2+} in these systems. These above fluorescence titration results confirmed that sample **5** possessed the sensing abilities for sequentially detecting Co^{2+}-Hg^{2+}-Cu^{2+}, which was reported for the first time. In addition, the influences of pH on fluorescence intensities of sample **5** with ions were investigated as shown in Figure S9, exhibiting a reasonable stability of fluorescence intensity between pH = 6 and 10.

3.7 The sensing mechanism

The stoichiometric ratios of sample **5** for Co^{2+}, Hg^{2+} and Cu^{2+} were investigated by the Job's plots as shown in Figure S10-12. It can be seen that the break points for fluorescence intensities were at 0.33, suggesting the 2:1 binding stoichiometric ratios of sample **5** for these metallic ions. Moreover, the MS spectrum of sample **5** with excess Cu^{2+}, Co^{2+} and Hg^{2+} were examined as shown in Figure 11, Figure S13 and S14, respectively. The strong peaks at *m/z* of 805.796, 400.380 and 941.629 were in accordance with the molecular weight of 2M+Cu^{2+}, (2M+Co^{2+})/2 and 2M+Hg^{2+} certainly supporting the 2:1 binding stoichiometric ratio again.

The contrast ^{1}H NMR spectra of sample **5** with Cu^{2+} were investigated to study the binding behaviour. As shown in Figure 12, the proton signals displayed obvious changes after binding Cu^{2+}. Especially, the protons of OH groups disappeared and the protons of CH=N groups displayed obvious shifts to low field, indicating the Cu^{2+} was binded in the cavity composed of N and O functional groups as inserted in Figure 12. Furthermore, the binding constant K_a was calculated by Benesi-Hildebrand equation (FigureS15-S17). The K_a values exhibited the order of Co^{2+} (4.06×10^{11}) < Hg^{2+} (2.23×10^{13}) < Cu^{2+} (2.87×10^{13}), which agreed with the changes of fluorescence of sample **5** in the presence of Co^{2+}, Hg^{2+} and Cu^{2+}. Thus, the whole sensing mechanism could be elucidated as Figure 13.

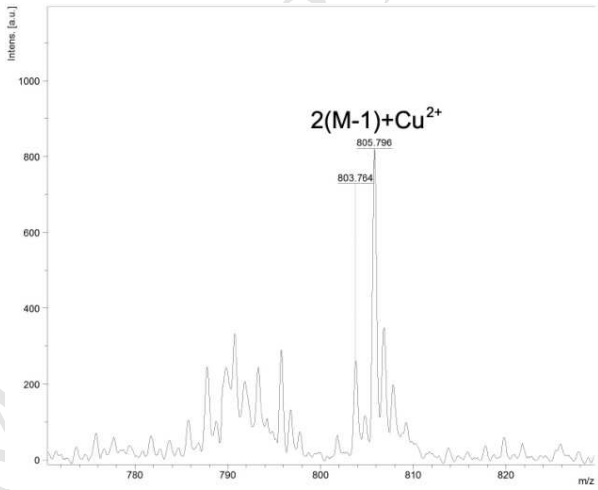

Figure 11. The mass spectrum of sample **5** with excess Cu^{2+}

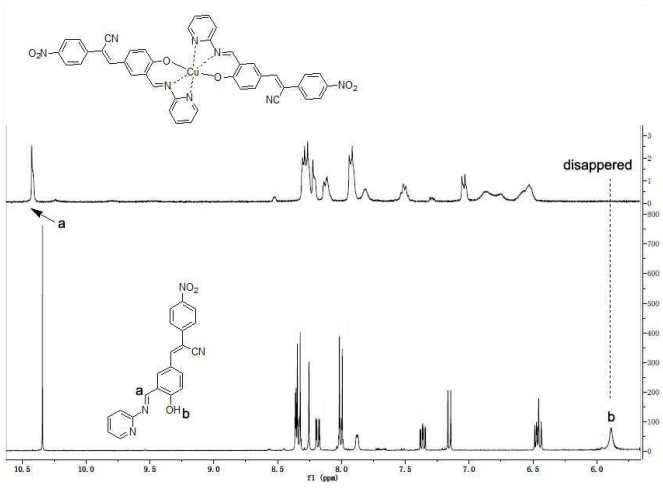

Figure 12. The contrast ^{1}H NMR spectra of sample **5** and sample **5** with Cu^{2+}

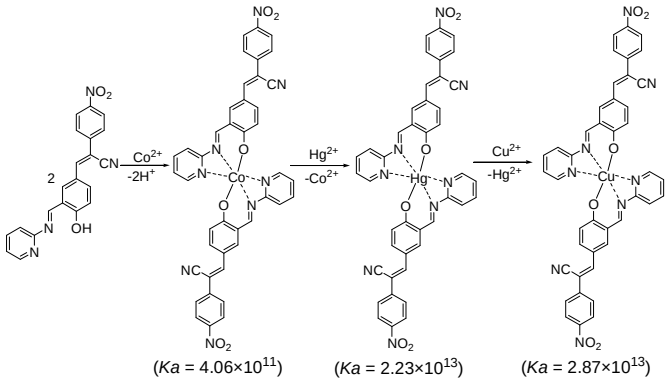

Figure 13. The sequentially sensing mechanism of sample **5** for Co^{2+}, Hg^{2+} and Cu^{2+}

3.8 Application in test paper

Test paper is the convenient method for the application of ion detection due to its portable and responsive peculiarities. Therefore, the test paper of sample **5** was obtained by tailoring filter paper into strips and immersed in 1 mM of sample **5** THF solution for 1 h. After drying in air, all test papers were fixed in the circular eyelet template. Furthermore, three drops of 0.1 mM solutions (H_2O/THF = 99:1), containing none, Ag^+, Al^{3+}, Ba^{2+}, Na^+, Pb^{2+}, Ca^{2+}, Cd^{2+}, Zn^{2+}, K^+, Fe^{3+}, Ni^{2+}, Li^+, Hg^{2+}, Bi^{3+}, Co^{2+}, Cu^{2+}, Mg^{2+} and Cr^{2+}, respectively, were added to the test papers. As shown in Figure 14, there was no color change for most of ions except for Co^{2+} and Cu^{2+}, indicating the sensing abilities for Co^{2+} and Cu^{2+}. Moreover, the sequentially sensor of test paper for Co^{2+}-Hg^{2+}-Cu^{2+} was studied. As shown in Figure 15, after adding Co^{2+} on test paper, the strong red fluorescence of tested paper (A) turned into no luminescence (B). Further dropping other metallic ions on test paper, the test paper still maintained no luminescence (C) except Hg^{2+}(D) exhibiting strong red fluorescence again. Further dropping Cu^{2+} on tested paper, the fluorescence quenched once more. These color changes of tested paper were in accordance with the fluorescence studies in solution, indicating the good application prospect of sample **5** for sensing Co^{2+}-Hg^{2+}-Cu^{2+} sequentially.

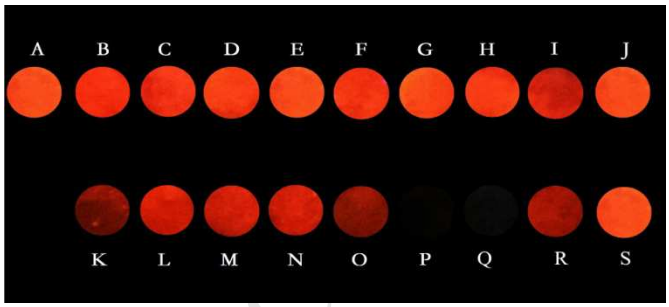

Figure 14. Fluorescence photographs of the test papers containing different species under UV light (365 nm). A = None, B = Ag^+, C = Al^{3+}, D = Ba^{2+}, E = Na^+, F = Pb^{2+}, G = Ca^{2+}, H = Cd^{2+}, I = Zn^{2+}, J = K^+, K = Fe^{3+}, L = Ni^{2+}, M = Li^+, N = Hg^{2+},O = Bi^{3+}, P = Co^{2+}, Q = Cu^{2+}, R = Mg^{2+} and S = Cr^{2+}, respectively.

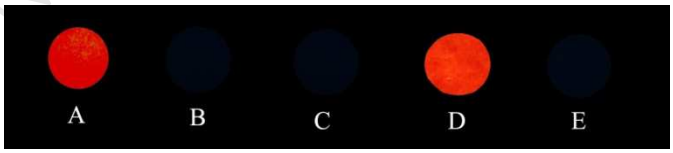

Figure 15. Photographs of the test papers, containing multiple species under UV light (365 nm). A = None, B = Co^{2+}, C = Co^{2+} and other tested ions except Hg^{2+}, D = Co^{2+} and Hg^{2+}, E = Co^{2+}, Hg^{2+} and Cu^{2+}.

3.9 Application in living cell imaging

In recent years, the living cell imaging of fluorescent probe exhibited the broad application prospects. A study of sample **5** was carried out by confocal laser scanning microscopy (CLSM) to explore imaging performance in biologic cells. According to the reported method of metabolic activity with MTT assay, sample **5** showed low

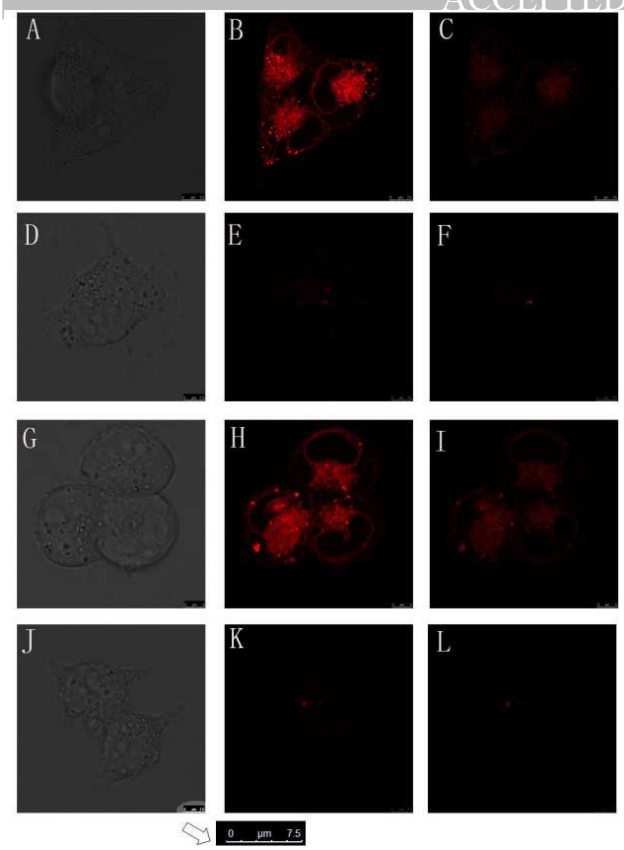

Figure 16. Confocal fluorescence images of MCF-7 cells before and after incubated with sample **5** (1.0×10^{-5} M) and/or ions. (A)-(C) sample **5**-MCF-7 cells; (D)-(F) sample **5**- MCF-7 cells- Co^{2+}; (G)-(I) sample **5**- MCF-7 cells- Co^{2+}-Hg^{2+}; (J)-(L) sample **5**- MCF-7 cells- Co^{2+}-Hg^{2+}-Cu^{2+}. Left images were bright field images, middle images were fluorescence images, and right images were the merged images of fluorescence and bright field. (λ_{ex} = 405 nm). The same scale bar for all images (as shown for image J).

biotoxicity with above 80% of the alive MCF-7 cell at concentration of 1.0×10^{-5} M for 24 h at 37 ^{o}C (Figure S18). The influence of concentrations on the cytotoxicity was studied, suggesting that the half-maximal inhibitory concentration (IC50) of sample **5** for MCF-7 cell was 29.3 μM (Figure S19). After adding ions of Co^{2+}-Hg^{2+}-Cu^{2+} in solution, the alive MCF-7 cell still attained 73%, 69% and 65%, respectively (Figure S20). Afterwards, sample **5** was tracked in MCF-7 cells by an hour of incubation. A bright orange-red fluorescence can be observed in the cell as shown in Figure 16. With the addition of Co^{2+}, the fluorescence became dim, further became bright again by adding Hg^{2+} and quenched finally by adding Cu^{2+}. These phenomena suggested that sample **5** possessed the good living cell imaging performance and could sense Co^{2+}-Hg^{2+}-Cu^{2+} sequentially in living system.

4. Conclusion

In summary, this work synthesized a red fluorescent sensor **5** based on AIE diphenylacrylonitrile with pyridine Schiff-base structure. Sample **5** exhibited good AIE property with strong red fluorescence at λ_{ex} = 620 nm and the Stokes shift was as large as 260 nm. The experiments of sensing series of metallic ions suggested that the fluorescence of sample **5** was quenched rapidly by adding Co^{2+} and Cu^{2+}. Moreover, the quenched fluorescence of sample **5** with Co^{2+} could be recovered by further adding Hg^{2+}, and then quenched again by adding Cu^{2+}. These results suggested the sequentially detecting abilities for Co^{2+}-Hg^{2+}-Cu^{2+} which was observed for the first time. The detection limits for Co^{2+}-Hg^{2+}-Cu^{2+} were 0.0937, 0.0221, and 0.0938 μM, respectively. The sensor mechanism of 2:1 stoichiometric ratios was proposed and confirmed by fluorescence titration, ^{1}H NMR and MS spectra. The test paper of sample **5** was prepared and applied successfully to the practical detection for Co^{2+}-Hg^{2+}-Cu^{2+} sequentially. The experiment of living cell imaging suggested

the good bioimaging performance of sample **5**. The fluorescence of living cells with sample **5** was also quenched by Co^{2+}, restored by further adding Hg^{2+}, and quenched finally in presence of Cu^{2+}, implying the good application prospect in detecting Co^{2+}-Hg^{2+}-Cu^{2+} for living body environment.

Acknowledgment. Financial support from the National Natural Science Foundation of China (No: 21406036), Fujian Natural Science Foundation of China (No. 2017J01571), Fujian Science and Technology Project (No. 2019N0010), Fuzhou science and technology project (2018-G-44), and Undergraduate innovation program of FJNU (2019) were greatly acknowledged.

References

[1] Siegel FR, Environmental Geochemistry of Potentially Toxic Metals, Springer, Berlin Heidelberg, Berlin, 2002.

[2] Kobielska PA, Howarth AJ, Farha OK, Nayak S. Metal-organic frameworks for heavy metal removal from water. Coordin Chem Rev 2018;358:92-107.

[3] Navas-Acien A, Selvin E, Sharrett AR, Calderon-Aranda E, Silbergeld E, Guallar E. Lead, cadmium, smoking, and increased risk of peripheral arterial disease. Circulation 2004;109:196-3201.

[4] Mozaffarian D, Shi P, Morris JS, Spiegelman D, Grandjean P, Siscovick DS, Willett WC, Rimm EB. Mercury exposure and risk of cardiovascular disease in two U.S. Cohorts. N Engl J Med 2011;364:1116-1125.

[5] Clarkson TW, Magos L, Myers GJ. The toxicology of mercury - Current exposures and clinical manifestations. N Engl J Med 2003;349:1731-1737.

[6] Salazar MT, Smith TK, Harris A. High-performance liquid chromatographic method for determination of biogenic amines in feedstuffs, complete feeds, and animal tissues. J Agric Food Chem 2000;48:1708-1712.

[7] Zhang Y, Peng C, Ma X, Che Y, Zhao J. Fluorescent and photoconductive nanoribbons as a dual-mode sensor for selective discrimination of alkyl amines versus aromatic amines. Chem Commun 2015;51:15004-15007.

[8] Feuster EK, Glass TE, Detection of amines and unprotected amino acids in aqueous conditions by formation of highly fluorescent iminium ions. J Am Chem Soc 2003;125:16174-16175.

[9] Takagai Y, Nojiri Y, Takase T, Hinze WL, Butsugan M, Igarashi S. "Turn-on" fluorescent polymeric microparticle sensors for the determination of ammonia and amines in the vapor state. Analyst 2010;135:1417-1425.

[10] Longstreet AR, Jo M, Chandler RR, Hanson K, Zhan N, Hrudka JJ, Mattoussi H, Shatruk M, Mcquade DT. Ylidenemalononitrile enamines as fluorescent "turn-on" indicators for primary amines. J Am Chem Soc 2014;136:15493−15496.

[11] Dong L, Deng C, He C, Shi L, Fu Y, Zhu D, Cao H, He Q, Cheng J. Highly sensitive vapor detection of amines with fluorescent conjugated polymer: A novel lasing turn-on sensory mechanism. Sens Actuators B 2013;180:28-34.

[12] Venkateswarulu M, Gaur P, Koner RR. Sensitive molecular optical material for signaling primary amine vapors. Sens Actuators B 2015;210:144-148.

[13] McGrier PL, Solntsev KM, Miao S, Tolbert LM, Miranda OR, Rotello VM, Bunz UHF. Hydroxycruciforms:

Amine-responsive fluorophores. Chem Eur J 2008;14:4503-4510.

[14] Mei J, Huang Y, Tian H. Progress and trends in AIE-based bioprobes: A brief overview. ACS Appl Mater Interfaces 2018;10:12217-12261.

[15] Lincoln R, Greene LE, Zhang W, Louisia S, Cosa G. Mitochondria alkylation and cellular trafficking mapped with a lipophilic BODIPY-acrolein fluorogenic probe. J Am Chem Soc 2017;139:16273-16281.

[16] Shie J, Liu Y, Lee Y, Lim C, Fang J, Wong C. An azido-BODIPY probe for glycosylation: Initiation of strong fluorescence upon triazole formation. J Am Chem Soc 2014;136:9953-9961.

[17] Sivaraman G, Iniya M, Anand T, Kotla NG, Sunnapu O, Singaravadivel S, Gulyani A, Chellappa D. Chemically diverse small molecule fluorescent chemosensors for copper ion. Coordin Chem Rev 2018;357:50-104.

[18] Rosenthal J, Lippard SJ. Direct detection of nitroxyl in aqueous solution using a tripodal copper(II) BODIPY complex. J Am Chem Soc 2010;132:5536-5537.

[19] Kuo S, Li H, Wu P, Chen C, Huang Y, Chan Y. Dual colorimetric and fluorescent sensor based on semiconducting polymer dots for ratiometric detection of lead ions in living cells. Anal Chem 2015;87:4765-4771.

[20] Li Y, Liu Y, Zhou H, Chen W, Mei J, Su J. Ratiometric Hg^{2+}/Ag^{+} probes with orange red-white-blue fluorescence response constructed by integrating vibration-induced emission with an aggregation-induced emission motif. Chem Eur J 2017;23:9280-9287.

[21] Uçuncu M, Emrullahoglu M. A BODIPY-based reactive probe for the detection of Au(III) species and its application to cell imaging. Chem Commun 2014;50:5884-5887.

[22] Luo J, Xie Z, Lam JW, Cheng L, Chen H, Qiu C, Kwok HS, Zhan X, Liu Y, Zhu D, Tang BZ. Aggregation-induced emission of 1-methyl-1,2,3,4,5-pentaphenylsilole. Chem Commun 2001;14:1740-1743.

[23] Yu X, Chen H, Shi X, Albouy P, Guo J, Hu J, Li M. AIE fluorescent gelators with thermo-, mechano-, and vapochromic properties. Mater Chem Front 2018;2:2245-2249.

[24] Jiang S, Qiu J, Chen Y, Guo H, Yang F. Luminescent columnar liquid crystals based on AIE tetraphenylethylene with hydrazone groups bearing multiple alkyl chains. Dyes Pigm 2018;159:533-541.

[25] Lin LB, Guo HY, Fang XT, Yang FF. Novel AIE columnar liquid crystals: the influence of the number of diphenylacrylonitrile groups on the mesomorphic and fluorescence properties. RSC Adv 2017;7:20172-20177.

[26] Guo HY, Lin LB, Qiu JB, Yang FF. Phenylacrylonitrile-bridging triphenylene dimers: the columnar liquid crystals with high fluorescence in both solid state and solution. RSC Adv 2017;7:53316-53322.

[27] Nie H, Chen B, Zeng J, Xiong Y, Zhao Z, Tang B. Excellent n-type light emitters based on AIE-active silole derivatives for efficient simplified organic light-emitting diodes. J Mater Chem C 2018;6:3690-3698.

[28] Lee WWH, Zhao Z, Cai Y, Xu Z, Yu Y, Xiong Y, Kwok RTK, Chen Y, Leung NLC, Ma D, Lam JWY, Qin A, Tang B. Facile access to deep red/near-infrared emissive

AIEgens for efficient non-doped OLEDs. Chem Sci 2018;9:6118-6125.

[29] Shi H, Zhang X, Gui C, Wang S, Fang L, Zhao Z, Chen S, Tang BZ. Synthesis, aggregation-induced emission and electroluminescence properties of three new phenylethylene derivatives comprising carbazole and (dimesitylboranyl) phenyl groups. J Mater Chem C 2017;5:11741-11750.

[30] Mei J, Leung NLC, Kwok RTK, Lam JWY, Tang BZ. Aggregation-induced emission: Together we shine, united we soar! Chem Rev 2015;115:11718-11940.

[31] Mei J, Hong Y, Lam JWY, Qin A, Tang Y, Tang BZ. Aggregation-induced emission: The whole is more brilliant than the parts. Adv Mater 2014;26:5429-5479.

[32] Jiang J, Qiu J, Lin L, Guo H, Yang F. Columnar self-assembly of tetraphenylethylene with multiple cholesterol units: Synthesis, mesophase and circularly polarized luminescence based on chiral transfer. Dyes Pigm 2019;163, 363-370.

[33] Chatterjee A, Banerjee M, Khandare DG, Gawas RU, Mascarenhas SC, Ganguly A, Gupta R, Joshi H. Aggregation-induced emission-based chemodosimeter approach for selective sensing and imaging of Hg(II) and methylmercury species, Anal Chem 2017;89:12698-12704.

[34] Huang X, Gu X, Zhang G, Zhang D. A highly selective fluorescence turn-on detection of cyanide based on the aggregation of tetraphenylethylene molecules induced by chemical reaction. Chem Commun 2012;48:12195-12197.

[35] Gong W, Aldred MP, Zhang G, Li C, Zhu M. Aggregation-induced emission logic gates based on metal ion sensing of phenanthroline-tetraphenylethene conjugates. J Mater Chem C 2013;1:7519-7525.

[36] Qiu J, Chen Y, Jiang S, Guo H, Yang F. A fluorescent sensor based on aggregation-induced emission: Highly sensitive detection for hydrazine and application in living cell imaging. Analyst 2018;143:4298-4305.

[37] Qiu J, Chen Y, Jiang S, Guo H, Yang F. An AIE and FRET-based BODIPY sensor with large Stoke shift: Novel pH probe exhibiting application in CO_3^{2-} detection and living cell imaging. Dyes Pigm 2018;157:351-358.

[38] Kang M., Gu X, Kwok RTK, Leung CWT, Lam JWY, Li F, Tang BZ. A near-infrared AIEgen for specific imaging of lipid droplets. Chem Commun 2016;52:5957-5960.

[39] Wang M, Zhang G, Zhang D, Zhu D, Tang BZ. Fluorescent bio/chemosensors based on silole and tetraphenylethene luminogens with aggregation-induced emission feature. J Mater Chem 2010;20:1858-1867.

[40] Donnier-Maréchal M, Abdullayev S, Bauduin M, Pascal Y, Fu M, He X, Gillon E, Imberty A, Kipnis E, Dessein R, Vida S. Tetraphenylethylene- based glycoclusters with aggregation- induced emission (AIE) properties as high-affinity ligands of bacterial lectins. Org Biomol Chem 2018;16:8804-8809.

[41] Kwok RTK, Leung CWT, Lam JWY, Tang BZ. Biosensing by luminogens with aggregation-induced emission characteristics. Chem Soc Rev 2015;44:4228-4238.

[42] Liu Y, Deng C, Tang L, Qin A, Hu R, Sun JZ, Tang BZ. Specific detection of D-glucose by a tetraphenylethene-based fluorescent sensor. J Am Chem Soc 2011;133:660-663

[43] Lan L, Niu Q, Guo Z, Liu H, Li T. Highly sensitive and fast responsive “turn-on” fluorescent sensor for selectively

sensing Fe^{3+} and Hg^{2+} in aqueous media based on an oligothiophene derivative and its application in real water samples. Sens Actuators B 2017;244:500-508.

[44] Vinkenborg JL, van Duijnhoven SMJ, Merkx M. Reengineering of a fluorescent zinc sensor protein yields the first genetically encoded cadmium probe. Chem Commun 2011;47:11879-11881.

[45] Ni Y, Wu J. Far-red and near infrared BODIPY dyes: synthesis and applications for fluorescent pH probes and bio-imaging. Org Biomol Chem 2014;12:3774-3791.

Novel red AIE fluorescence sensor was prepared with Stokes shift of 260 nm.

The sequentially detecting abilities for Co^{2+}-Hg^{2+}-Cu^{2+} was firstly observed.

It showed good bioimaging performance on living cell for sensing Co^{2+}-Hg^{2+}-Cu^{2+}.

The detection limits for Co^{2+}, Hg^{2+} and Cu^{2+} were 0.0937, 0.0221, and 0.0988 μM.

The sensor mechanism was confirmed as 2:1 stoichiometric ratio.